IOP FTC
IOP PUBLISHING JOURNAL OF PHYSICS A: MATHEMATICAL AND THEORETICAL
J. Phys. A: Math. Theor. **45** (2012) 302001 (9pp) doi:10.1088/1751-8113/45/30/302001

FAST TRACK COMMUNICATION

Riemann zeros in radiation patterns

M V Berry

H H Wills Physics Laboratory, University of Bristol, Tyndall Avenue,
Bristol BS8 1TL, UK

E-mail: asymptotico@physics.bristol.ac.uk

Received 8 June 2012, in final form 28 June 2012
Published 16 July 2012
Online at stacks.iop.org/JPhysA/45/302001

Abstract
Propagation into the far field changes initial waves into their Fourier transforms. This implies that the Riemann zeros could be observed experimentally in the radiation pattern generated by an initial wave whose Fourier transform is proportional to the Riemann zeta function on the critical line. Two such waves are examined, generating the Riemann $\Xi(t)$ function (pattern 1) and the function $\zeta(1/2 + \mathrm{i}t)/(1/2 + \mathrm{i}t)$ (pattern 2). For pattern 1, the radiation side lobes are probably too weak to allow detection of the zeros, but for pattern 2 the lobes are stronger, suggesting a feasible experiment.

PACS numbers: 02.10.De, 02.30.Gp, 02.30.Nw, 42.30.Kq, 42.25.Bs

(Some figures may appear in colour only in the online journal)

1. Introduction

As is well known, propagation of a wave from the near to the far field transforms an initial state into its Fourier transform. Explicitly, consider the transform pair

$$f(u) = \frac{1}{2\pi}\int_{-\infty}^{\infty} \mathrm{d}t\, g(t)\exp(\mathrm{i}tu), \tag{1.1}$$

and a wave $\psi(x,z)$ propagating in the plane according to the Helmholtz equation, with initial state

$$\psi(x,0) = f\left(\frac{x}{x_0}\right), \tag{1.2}$$

where x_0 is a length, specifying the spatial scale. Then, if the wavenumber (2π/wavelength) is k, the wave at x, z can be written, exactly, as a superposition of plane waves:

$$\psi(x,z) = \frac{1}{2\pi}\int_{-\infty}^{\infty} \mathrm{d}t\, g(t)\exp\left(\mathrm{i}\left(t\frac{x}{x_0} + z\sqrt{k^2 - \frac{t^2}{x_0^2}}\right)\right). \tag{1.3}$$

(The sign of the square root is chosen so that contributions $|t| > kx_0$ represent evanescent waves.) In the far field $r = \sqrt{x^2 + z^2} \to \infty$, standard stationary-phase arguments give

$$\psi(r\sin\theta,\ r\cos\theta) \underset{r\to\infty}{\to} x_0\sqrt{\frac{k}{2\pi \mathrm{i} r}}\exp(\mathrm{i}kr)\cos\theta g(kx_0\sin\theta), \tag{1.4}$$

and hence the radiation intensity pattern

$$I(\theta) = |g(kx_0\sin\theta)|^2\ \cos^2\theta. \tag{1.5}$$

We will be dealing with functions for which $f(t)$ is real, so $g(t)^* = g(-t)$, i.e. $|g(t)| = |g(-t)|$.

Here the emphasis will be on the zeros $\pm t_n$, that is $g(\pm t_n) = 0$. These separate the side lobes of the radiation pattern. The zeros occur in directions θ_n, where

$$\sin\theta_n = \pm\frac{t_n}{kx_0}. \tag{1.6}$$

Thus, for given scale kx_0 of the initial wave, zeros that appear in the range of physical forward directions $|\theta| < \frac{1}{2}\pi$ are $\pm t_1$ to $\pm t_N$, where

$$t_N \approx kx_0. \tag{1.7}$$

Several functions $f(u)$ are known whose Fourier transforms vanish at the heights (imaginary parts) t_n of the complex zeros of the Riemann zeta function [1, 2]. Therefore implementation of any such $f(u)$ as the wave amplitude in an initial plane will lead to a far-field radiation pattern in which the intensity vanishes in directions (1.6) corresponding to the Riemann zeros. This raises the possibility of direct observation of the Riemann zeros in a physical system, for example in optics, where analytically specified waveforms can be sculpted using a spatial light modulator [3, 4]. In the following, the feasibility of such experiments will be explored for two Riemann-related functions $f(u)$, giving two different predicted radiation patterns.

Four preliminary remarks. First, we note that there is an alternative possibility for physically implementing a Fourier transform, as noted by Crandall [5, 6]. Let $f(u)$ be the spatial dependence of the initial state of a quantum system evolving in a harmonic-oscillator potential. After a certain time, corresponding to a $\pi/2$ rigid rotation in phase space, the state becomes $g(t)$: position u has evolved into momentum t. Second, the existence of functions $f(u)$ with Fourier transforms vanishing at the Riemann zeros has led to several mathematical explorations [7–10] of Fourier transforms with real zeros, motivated by the Riemann hypothesis [1, 2], which states that all t_n are real. Third, I emphasize that this possible connection with physics is not intended to suggest any strategy for proving or disproving the Riemann hypothesis; indeed, it will be convenient to assume that all t_n are real. Fourth, as a referee has pointed out, a precedent for using radiation to illustrate a fundamental question is the dispersion that would result if the photon had non-zero mass [11].

2. Radiation pattern 1

The Riemann Ξ function,

$$g(t) = \Xi(t) = -\tfrac{1}{2}\left(t^2 + \tfrac{1}{4}\right)\pi^{-\left(\frac{1}{4}+\frac{1}{2}\mathrm{i}t\right)}\Gamma\left(\tfrac{1}{4} + \tfrac{1}{2}\mathrm{i}t\right)\zeta\left(\tfrac{1}{2} + \mathrm{i}t\right), \tag{2.1}$$

is known [1] to be an even entire function, real for real t, vanishing only at the complex Riemann zeros (the trivial zeros, that is, $\zeta(-2n) = 0$, are cancelled by the poles of the gamma function, and the pole $\zeta(1) = \infty$ is cancelled by the factor $t^2+1/4$). In terms of the zeros, $\Xi(t)$ can be written explicitly in terms of the Hadamard product

$$\Xi(t) = \tfrac{1}{2}\prod_{n=1}^{\infty}\frac{t_n^2 - t^2}{t_n^2 + \frac{1}{4}}, \tag{2.2}$$

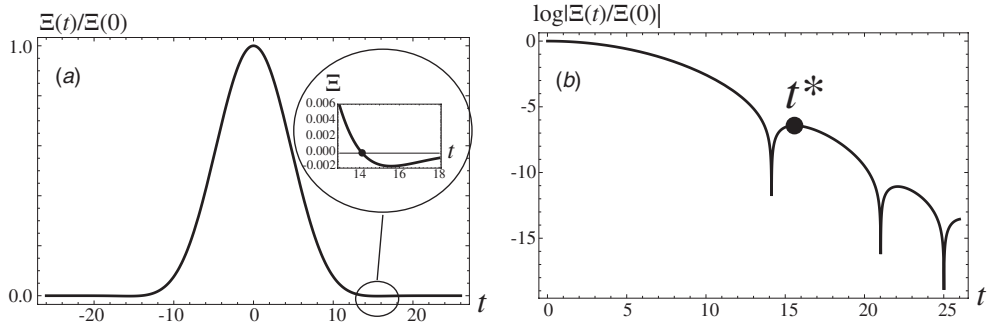

Figure 1. (*a*) Ξ(t) (equation (2.2)) with inset showing first Riemann zero; (*b*) $\log|\Xi(t)|$, showing position t^* of maximum between first two zeros.

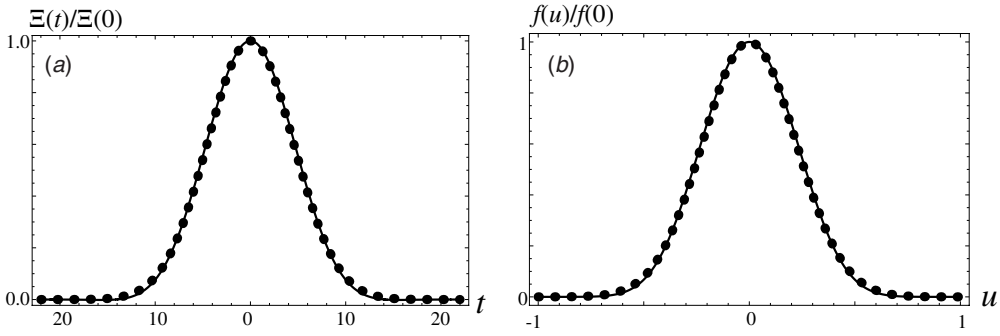

Figure 2. (*a*) Ξ(t) and (*b*) $f(u)$ (equation (2.3)) (full curves) compared with Gaussian approximations with the same rms widths (dotted curves).

whose convergence is examined in the appendix. As figure 1 illustrates, $\Xi(t)$ decays rapidly as t increases, and takes very small values between the zeros.

The function $f(u)$, of which $\Xi(t)$ is the Fourier transform, is [1, 6]

$$f(u) = \sum_{n=1}^{\infty} \left(4\pi^2 n^4 \exp\left(\tfrac{9}{2}u\right) - 6\pi n^2 \exp\left(\tfrac{5}{2}u\right)\right) \exp(-\pi n^2 \exp(2u)). \tag{2.3}$$

Obviously this is real for real u, and application of the Poisson sum formula shows that, naive appearance notwithstanding, the function is even: $f(u) = f(-u)$.

Figure 2(*b*) shows the function $f(u)$. At the resolution shown, it looks similar to $\Xi(t)$ in figure 2(*a*). Moreover, both are closely fitted by Gaussians. A measure of the closeness can be described in terms of the rms widths

$$w_u = \sqrt{\frac{\int_0^\infty \mathrm{d}u u^2 f^2(u)}{\int_0^\infty \mathrm{d}u f^2(u)}} = 0.156\,7804, \quad w_t = \sqrt{\frac{\int_0^\infty \mathrm{d}t t^2 g^2(t)}{\int_0^\infty \mathrm{d}t g^2(t)}} = 3.194\,9280, \tag{2.4}$$

giving the uncertainty product

$$w_u w_t = 0.500\,902. \tag{2.5}$$

This is very close to the value 1/2 of the minimum-uncertainty Fourier pair in which $f(u)$ and $g(t)$ would be exactly Gaussian. But of course $f(u)$ and $\Xi(t)$ are not Gaussians, and it

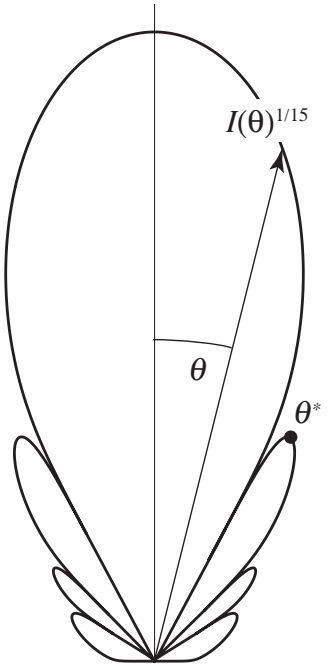

Figure 3. Radiation pattern 1, given by (1.5) with $\Xi(t)$ (equation (2.1)), for $kx_0 = 30$, as a polar plot of $I(\theta)^{1/15}$, showing first three Riemann zeros.

is precisely the deviations, especially the zeros of $\Xi(t)$, that are of interest here. This further illustrates the known extreme delicacy of analytic behaviour of the zeta function.

Figure 3 shows the radiation pattern corresponding to $\Xi(t)$, for a value kx_0 chosen to display the first three Riemann zeros. These zeros would be invisible on a simple polar plot of $I(\theta)$, because $\Xi(t)$ decays so rapidly that the polar plot would be dominated by a thin needle near $\theta = 0$. To see the side lobes, and the zeros separating them, it was necessary to reduce the variation of $\Xi(t)$ by plotting $I(\theta)^{1/15}$ rather than $I(\theta)$ itself. A measure of the rapid decay is given by the intensity in the direction θ^* of the first side lobe, corresponding to the maximum of $|\Xi|$ between zeros t_1 and t_2:

$$\frac{I(\theta^*)}{I(0)} = 2.6 \times 10^{-6}. \tag{2.6}$$

This is small, so observation of the zeros, as envisaged here, could be difficult: even with dynamic range sufficient to detect the intensity in the side lobes, noise could be a problem. Therefore we now move to the second function implementing the Riemann zeros, for which the ratio is much larger.

3. Radiation pattern 2

This is the complex function

$$g(t) = \frac{\zeta\left(\frac{1}{2} + \mathrm{i}t\right)}{\frac{1}{2} + \mathrm{i}t}, \tag{3.1}$$

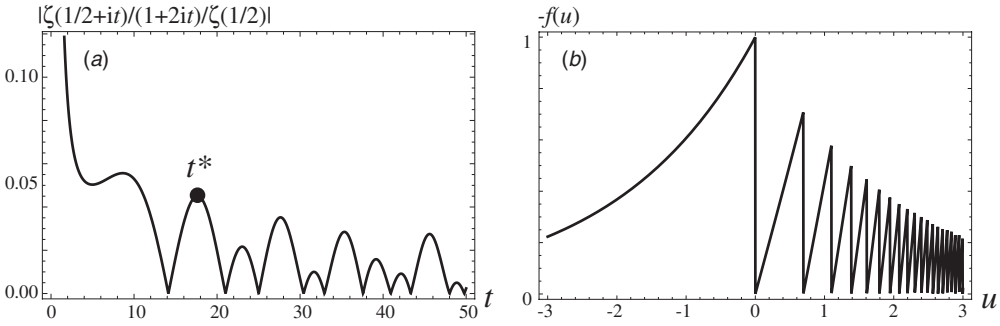

Figure 4. (*a*) $|\zeta(1/2{+}\mathrm{i}t)/\,(1/2{+}\mathrm{i}t)|$ and (*b*) $f(u)$ (equation (3.2)) for van der Pol realization [12] of the Riemann zeros.

whose modulus—an even function of t—is shown in figure 4(*a*). As can be seen, it decays more slowly than $\Xi(t)$ (figure 1), and the Riemann zeros are more evident.

This $g(t)$ is a complex function with $|g(t)|$ even, so the Fourier transform $f(u)$ is real but not even. It was shown by van der Pol [12] to be

$$f(u) = \exp\left(-\tfrac{1}{2}u\right)\mathrm{floor}(\exp u) - \exp\left(\tfrac{1}{2}u\right). \tag{3.2}$$

This function is illustrated in figure 4(*b*). This representation, surprising at first encounter, can easily be confirmed by evaluating the Fourier transform of $f(u)$ after separating the range of integration into intervals $\log n \leqslant u \leqslant \log(n{+}1)$. It also follows from

$$\zeta(s) = \frac{1}{1-s}\left(-s + \sum_{n=1}^{\infty} n^{1-s}\left(1 - \left(1+\frac{s}{n}\right)\left(1+\frac{1}{n}\right)^{-s}\right)\right), \tag{3.3}$$

which itself reduces to the familiar Dirichlet series $\zeta(s) = \sum_{n=1}^{\infty} n^{-s}$ for Re $s{>}1$ and converges inside the critical strip $0 <$ Re $s < 1$.

Figure 5 shows the radiation pattern corresponding to that shown in figure 3 for $\Xi(t)$. Since the intensity variations are more moderate, the side lobes and zeros can be discerned with a more modest scaling in the polar plot: $I(\theta)^{1/3}$ rather than $I(\theta)^{1/15}$ as in figure 3. Correspondingly, the intensity of the first side lobe is much larger than in (2.6):

$$\frac{I(\theta^*)}{I(0)} = 0.002\,03. \tag{3.4}$$

This is still small, but has a better chance of being detectable experimentally.

In practice it is impossible to create an initial wave over the entire range $-\infty < x < +\infty$. Therefore it is important to estimate whether the inevitable truncation of $f(u)$ will spoil the detection of the zeros. With a sharp cutoff, that is

$$f_N(u) = f(u)\Theta(\log N - |x|) \tag{3.5}$$

(in which Θ is the unit step), the radiation pattern will be determined not by $g(t)$ in (3.1) but by the transform

$$g_N(t) = \int_{-\infty}^{\infty} \mathrm{d}u f_N(u)\exp(-\mathrm{i}tu) = \frac{\zeta\left(\frac{1}{2} - \mathrm{i}t\right)}{\frac{1}{2} - \mathrm{i}t} - \Delta_N(t) \tag{3.6}$$

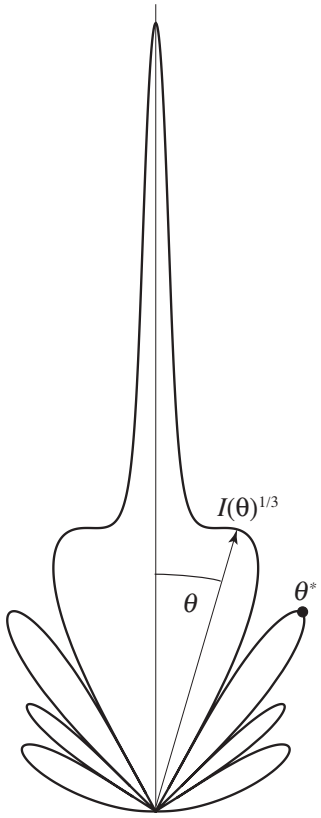

Figure 5. Radiation pattern 2, given by (1.5) with $\zeta(1/2+it)/(1/2+it)$ (equation (3.1)), for $kx_0 = 30$, as a polar plot of $I(\theta)^{1/3}$, showing first three Riemann zeros.

of $f_N(u)$. Simple asymptotics (involving averaging over the sawteeth for $u \gg 1$) gives the truncation error as

$$\Delta_N(t) = \int_{\log N}^{\infty} du \exp(-iut) f(u) + \int_{-\infty}^{-\log N} du \exp(-iut) f(u)$$
$$\times \underset{N\gg\frac{t}{2\pi},N\gg 1}{\approx} -\frac{1}{\sqrt{N}} \left(\frac{\exp(it\log N)}{\frac{1}{2}-it} + \frac{\exp(-it\log N)}{2\left(\frac{1}{2}+it\right)} \right). \tag{3.7}$$

As comparison of the thick and dotted curves in figure 6 illustrates, reasonable truncation introduces some undulations in the radiation pattern but does not obscure the zeros. And the thin curve in figure 6, calculated for a more brutal truncation, shows the accuracy of the approximate tail (3.7).

The functions $f(u)$ and $g(t)$ in this section, defined by (3.1) and (3.2), are very far from a minimum-uncertainty Fourier pair. The reason is that although the $f(u)$ width, defined similarly to (2.4), is finite, namely

$$w_u = \sqrt{\frac{\int_{-\infty}^{\infty} du u^2 f^2(u)}{\int_{-\infty}^{\infty} du f^2(u)}} = 1.455\ldots, \tag{3.8}$$

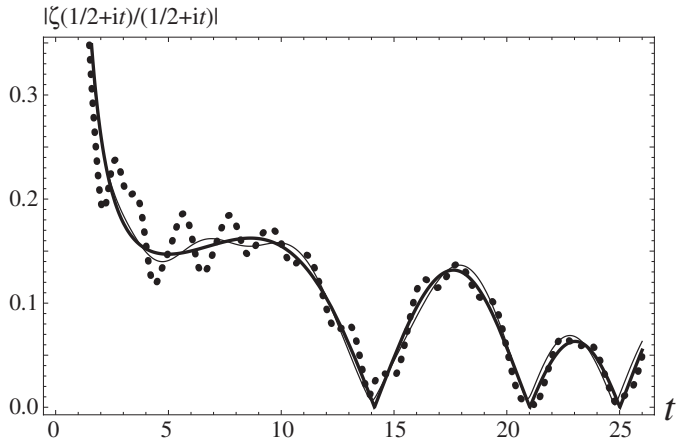

Figure 6. Truncated zeta function. The full curve shows the exact $g(t)$ from (3.1); the dotted curve shows the truncation $g_N(t)$ given by (3.6), for $N = 20$ (i.e. the truncation $|u| \leqslant \log 20 = 2.996$); the thin curve shows the truncation plus the approximate tail $\Delta_N(t)$ (equation (3.7)) for $N = 5$ (i.e. the truncation $|u| \leqslant \log 5 = 1.609$).

the corresponding $g(t)$ width, that is, the width of the radiation pattern, diverges like the integral of $\left|\zeta\left(\frac{1}{2} + \mathrm{i}t\right)\right|^2$. Nevertheless, the total power in the radiation pattern is finite; in fact [6]

$$\int_{-\infty}^{\infty} \mathrm{d}t\,|g(t)|^2 = \int_{-\infty}^{\infty} \mathrm{d}t \left|\frac{\zeta\left(\frac{1}{2} + \mathrm{i}t\right)}{\frac{1}{2} + \mathrm{i}t}\right|^2 = 2\pi \int_{-\infty}^{\infty} \mathrm{d}u\, f(u)^2$$
$$= 2\pi\,(\log 2\pi - \gamma) = 7.921\ldots. \tag{3.9}$$

4. Concluding remarks

The observation envisaged here would complement a remarkable old experiment by van der Pol [12]: instead of truncating $f(u)$ as in (3.5), the function (3.2) was periodized by cutting it round the periphery of a circular disk of paper (radius $= r_0 + \varepsilon f(N\theta/2\pi)$, where $\varepsilon \ll r_0$ and $N \gg 1$ are constants), which was then rotated rapidly and illuminated by a narrow beam of light, whose transmission was detected and the signal Fourier-transformed electronically. In this way, the lowest 25 Riemann zeros were identified.

If the diffraction experiment proposed here were carried out optically, a simplification would be to focus the radiation pattern onto a plane with a lens. Another possibility is to use microwaves or radio, and create the function $f(u)$ with a suitable antenna. With either, detecting as many as 25 zeros would be a challenge, even when based on the more promising pattern 2. But it is surely worth trying, if only to explore the intriguing possibility of seeing the Riemann zeros directly, simply by allowing a suitably sculpted wave to propagate.

Acknowledgment

I thank the Physics and Mathematics Departments of Portland State University for generous hospitality while the first draft of this paper was written.

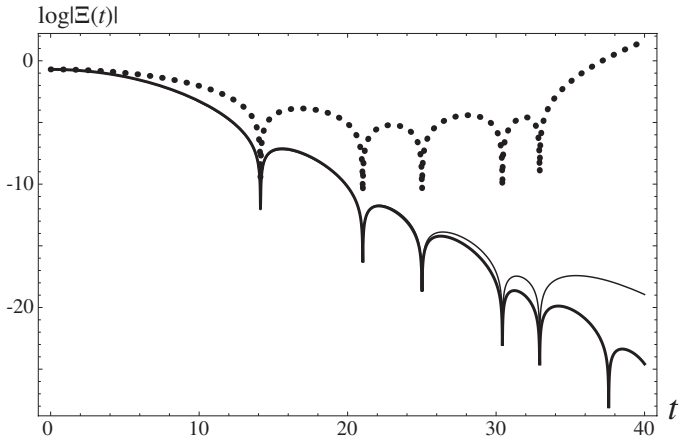

Figure A.1. Riemann function $\Xi(t)$ (thick curve), compared with Hadamard product truncated at $N = 5$ (dotted curve), and truncation at $N = 5$ with approximate tail (A.4) (thin curve). Note that the approximations fail beyond $t = t_5 = 32.94$, as expected, because zeros $n > 5$ are not included.

Appendix. Convergence of the product (2.2)

If we want to represent the first $\Xi(t)$ accurately including the zeros $t \leqslant t_N$, using the product (2.2), it is obviously necessary to include at least the first N factors. To estimate the collective effect of the remaining factors on $\Xi(t)$ for $t \leqslant t_N$, we write the product as

$$\Xi(t) = \tfrac{1}{2}\prod_{n=1}^{N}\frac{t_n^2 - t^2}{t_n^2 + \frac{1}{4}}P_N(t). \tag{A.1}$$

Elementary manipulations give the tail as

$$\begin{aligned} P_N(t) = \prod_{N+1}^{\infty}\frac{t_n^2 - t^2}{t_n^2 + \frac{1}{4}} &= \exp\left(\sum_{N+1}^{\infty}\left(\log\left(1 - \frac{t^2}{t_N^2}\right) - \log\left(1 + \frac{1}{4t_N^2}\right)\right)\right) \\ &= \exp\left(-\sum_{m=1}^{\infty}\frac{1}{m}\left(t^{2m} - \frac{(-1)^m}{4^m}\right)\sum_{N+1}^{\infty}\frac{1}{t_n^{2m}}\right). \end{aligned} \tag{A.2}$$

To estimate this for $N \gg 1$ we can replace the sums over the zeros by integrals over their known [1] asymptotic density. Thus

$$\sum_{N+1}^{\infty}\frac{1}{t_n^{2m}} \approx \frac{1}{2\pi}\int_{t_{N+1}}^{\infty}\mathrm{d}t\,\frac{\log(t/2\pi)}{t^{2m}} = \frac{\log\left(\mathrm{e}\left(\frac{t_{N+1}}{2\pi}\right)^{2m-1}\right)}{2\pi\,(2m-1)^2 t_{N+1}^{2m-1}}. \tag{A.3}$$

The sum over m in (A.2) can now be evaluated analytically, but it suffices to consider just the leading order for the tail, namely

$$P_N(t) \approx \exp\left(-\left(t^2 + \frac{1}{4}\right)\frac{\log\left(\frac{t_N\mathrm{e}}{2\pi}\right)}{2\pi t_N} + O\left(\frac{t^4\log t_N}{t_N^3}\right)\right). \tag{A.4}$$

Figure A.1 shows the dramatic improvement in the truncated product for $t < t_N$ when the leading order tail is included.

References

[1] Edwards H M 1974 *Riemann's Zeta Function* (New York: Academic)
[2] Borwein P, Choi S, Rooney B and Weirathmueller A 2008 *The Riemann Hypothesis: A Resource for the Aficionado and Virtuoso Alike* (Berlin: Springer)
[3] Slinger C, Cameron C and Stanley M 2005 Computer-generated holography as a generic display technology *Computer* **38** 46–53
[4] Savage N 2009 Digital spatial light modulators *Nature Photon.* **3** 170–2
[5] Crandall R E 1991 *Mathematica for the Sciences* (Redwood City, CA: Addison-Wesley)
[6] Borwein J M, Bradley D M and Crandall R E 2000 Computational strategies for the Riemann zeta function *J. Comput. Appl. Math.* **121** 247–96
[7] Polya G 1923 On the zeros of an integral function represented by Fourier's integral *Messenger Math.* **52** 185–8
[8] Polya G 1926 On the zeros of certain trigonometric integrals *J. Lond. Math. Soc.* **1** 98–99
[9] Newman C M 1976 Fourier transforms with only real zeros *Proc. Am. Math. Soc.* **61** 245–51
[10] Cardon D A 2004 Fourier transforms having only real zeros *Proc. Am. Math. Soc.* **133** 1349–56
[11] Crandall R E and Wheeler N A 1984 Klein–Gordon radio and the problem of photon mass *Nuovo Cimento* B **80** 231–42
[12] van der Pol B 1947 An electro-mechanical investigation of the Riemann zeta function in the critical strip *Bull. Am. Math. Soc.* **53** 976–81